INTERFEROMETRIC MAPPING OF GROUND DEFORMATION IN NISSYROS VOLCANO, AEGEAN SEA, DURING 1995-1996.

GANAS[1] ATHANASSIOS, LAGIOS[2] EVANGELOS, DIETRICH[3],. VOLKER. J., VASSILOPOULOU[2], SPIRIDOULA, HURNI[3], LORENZ, AND STAVRAKAKIS[1] GEORGE.

ABSTRACT

Nissyros is an active volcano in the south Aegean Sea, Greece. Deformation maps were produced using ERS C-band SAR image pairs acquired in 1995/96, over a time period of 279 days. This is the earlier deformation signal ever mapped on Nissyros. Results of the investigation clearly indicate significant off-caldera ground deformation. Surface uplift occurred in Mandraki area (NW Nissyros), and the affected area coincides with a particular geologic discontinuity, a normal fault that moved during the August 1997 5.5 Ms earthquake. Derived uplift rates are supported by the results of geodetic measurements (GPS).

ΠΕΡΙΛΗΨΗ

Η νήσος Νίσυρος είναι ένα ενεργό ηφαίστειο στο νοτιο-ανατολικό Αιγαίο πέλαγος. Στα πλαίσια ενός ευρωπαϊκού ερευνητικού προγράμματος κατασκευάσαμε χάρτες ανηγμένης παραμορφώσεως για τη Νίσυρο χρησιμοποιώντας την τεχνική της δορυφορικής συμβολομετρίας. Ο δορυφορικός χάρτης της περιόδου 1995-1996 αποτελεί την πρώτη απόδειξη αλλαγής σχήματος του ηφαιστείου εξ' αιτίας ανόδου μάγματος στον ανώτερο φλοιό. Οι μετρήσεις επιβεβαιώνονται από γεωδετικά δεδομένα επομένων ετών.

ΛΕΞΕΙΣ ΚΛΕΙΔΙΑ: Τηλεπισκόπιση, Ηφαιστειότητα, Συμβολομετρία, ERS, DEM, Νίσυρος.
KEY WORDS: Remote Sensing, Volcanism, Interferometry, ERS, DEM, Nissyros

INTRODUCTION

The Nissyros volcano is located at the southeastern end of the South Aegean Volcanic Arc at about 36.5 degrees North and 27.1 degrees East (Georgalas, 1962; Figure 1). Although the last volcanic activity on Nissyros dates back at least 25000 years, the present geodynamic activity encompasses high seismic unrest, widespread fumarolic activity, and recent gas and hydrothermal explosions (Papadopoulos *et al.,* 1998; Dietrich *et al.*, 1998). Earthquakes and steam blasts accompanied the most recent hydrothermal eruptions in 1871-1873 and 1887. Mudflows and hydrothermal vapors rich in CO_2 and H_2S were emitted from fracture zones that cut the caldera of the volcano and extend towards NNW through the vicinity of the village of Mandraki. The seismic unrest of the years 1995-1997 prompted us to initiate an interferometric study of the ground deformation using spaceborne data from the European satellites ERS1 and ERS2. Differential Interferometry has been an effective tool in mapping ground deformation of active volcanoes (e.g. Massonnet *et al.,* 1995, Lanari *et al.,* 1998; Lu *et al.,* 2000).

The ERS data were originated in the I-PAF facility in CEOS-SLCi format with dimensions 4900 pixels (range) by approximately 26500 rows (azimuth) resulting in ground resolution 7.9 metres in range - 3.98 metres in azimuth. The Pulse Repetition Frequency (PRF), a critical factor in data processing (Gens, 2000) for both satellites is 1679.902 Hz. The radar wavelength is 5.65 cm (frequency 5.3 GHz) and the antenna depression angle is 67 degrees during data acquisitions. The radar data were processed by EVInSAR, (1.2.1 version) produced by ATLANTIS (van der Kooij, *et al.,* 1997) on a Pentium III computer with 392 Mb RAM.

_____

1:Geodynamics Institute, National Observatory of Athens, PO Box 20048, 118 10 Athens, Greece. E-mail: aganas@gein.noa.gr
2:Space Applications Unit in Geosciences, University of Athens, Department of Geology, 157 84 Panepistimiopolis, Athens, Greece.
3:Institut of Mineralogy and Petrography, ETH, Sonneggstrasse 5, CH-8092 Zurich, Switzerland

Figure 1. Location map of the Nissyros volcano, Aegean Sea. The image to the right is a black-and-white space photograph of the Space Shuttle. The image shows in 2D the circular geometry of Nissyros and the caldera in the middle.
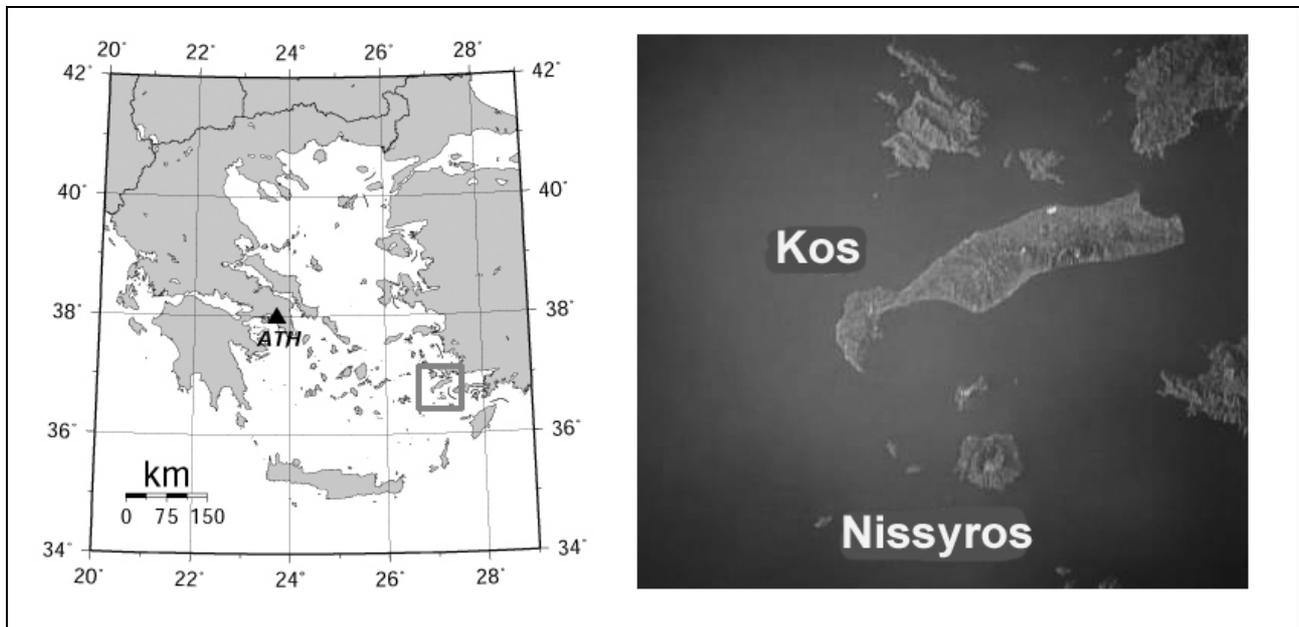
METHODOLOGY

The ODISSEO web Server of ESA (http://jupiter.esrin.esa.it/) was searched for the selection of suitable pairs for InSAR. Ten (10) images were selected and were delivered as Single Look Complex (SLCi) products. Two optimal scenes were selected for further analysis, namely orbits 5973 (11 June 1996) and 1965 (5 September 1995) of the ERS 2 satellite (Table 1). These scenes had temporal separation of 279 days which span the time period of increased seismicity rates while preserving adequate phase coherence. Locally there is a high level of correlation between the two ERS scenes; however, over most of the island the coherence remains at relatively low levels.

The orbital baselines (B) were: perpendicular B = -79.9 m, parallel B = -27.7 m. The orbital parameters of the two scenes were refined by more accurate estimations of the state vector positions as calculated by the DEOS (Scharroo *et al.*, 1998). We used the 2-pass method by eliminating topographic phase using an external DEM with a resolution of 2 metres. The DEM was produced by digitizing of the 1:5000 topographic maps of Nissyros provided by HMGS (Hellenic Military Geographical Service). The DEM was edited and corrected with field measurements by the Institute of Cartography, ETHZ at a final resolution of two (2) metres (Vassilopoulou and Hurni, 2001). This good quality had two implications: a) it provided ground control for the co-registration between master SAR scene-slant range projected DEM between 1-4 m and b) brought down the magnitude of the topographic artifact to 4m / 117 m (altitude of ambiguity *ha*) or 0.034 of a cycle or 1mm using Pair 1. All datasets were reprojected to the WGS84 datum, UTM zone 35.

Data processing starts with image co-registration analysis. This includes: a) Resampling of DEM to master SAR image b) Processing to distort the re-sampled DEM into the master SAR space creating foreshortening and layover distortions c) Fine coregistration of DEM to master SAR image using ground control points and d) Calculation and subtraction of topographic phase from the interferogram prior to interferogram enhancement. In step c) an advanced SAR image backscatter simulator is used to generate a simulated SAR image for use in fine coregistration of DEM to master. For example, the fine coregistration for the

Pair was done using 23 ground control points with root mean square errors along x=0.54 and along y=0.66 pixels. The phase difference is unwrapped using an iterative disk masking algorithm with controlled error propagation and error correction. The algorithm uses multiple tiling and seeding techniques, providing automatic masking of low coherence areas and automatic connection of residues. An unwrapping editor was also used to correct remaining errors. Data resampling is applied to reduce the amount of data to be phase unwrapped and give square dimensioned pixels in ground range.

_____

Table 1. Interferometric Pair Validation results. The first stage of SAR image processing after data input. Spectral overlap between two SAR scenes indicates amount of noise introduced to the phase difference of the two interferograms because of their bandwidths centered at different frequencies.

SAR Image	Sensor-Orbit	Date	Spatial Overlap	Range Spectral	Azimuth Spectral
Pair 1 – Master	ERS 2 – 5973	11-6-1996	96.91 %	92.71%	98.99%
Pair 1 – Slave	ERS 2 - 1965	5-9-1995			

Figure 2. The interferogram of Nissyros volcano spanning the period between orbits 5973 (11 June 1996) and 1965 (5 September 1995) of the ERS 2 satellite. Note the E-W strike of the first fringe (black arrow - blue to red colour change), that is across topography.
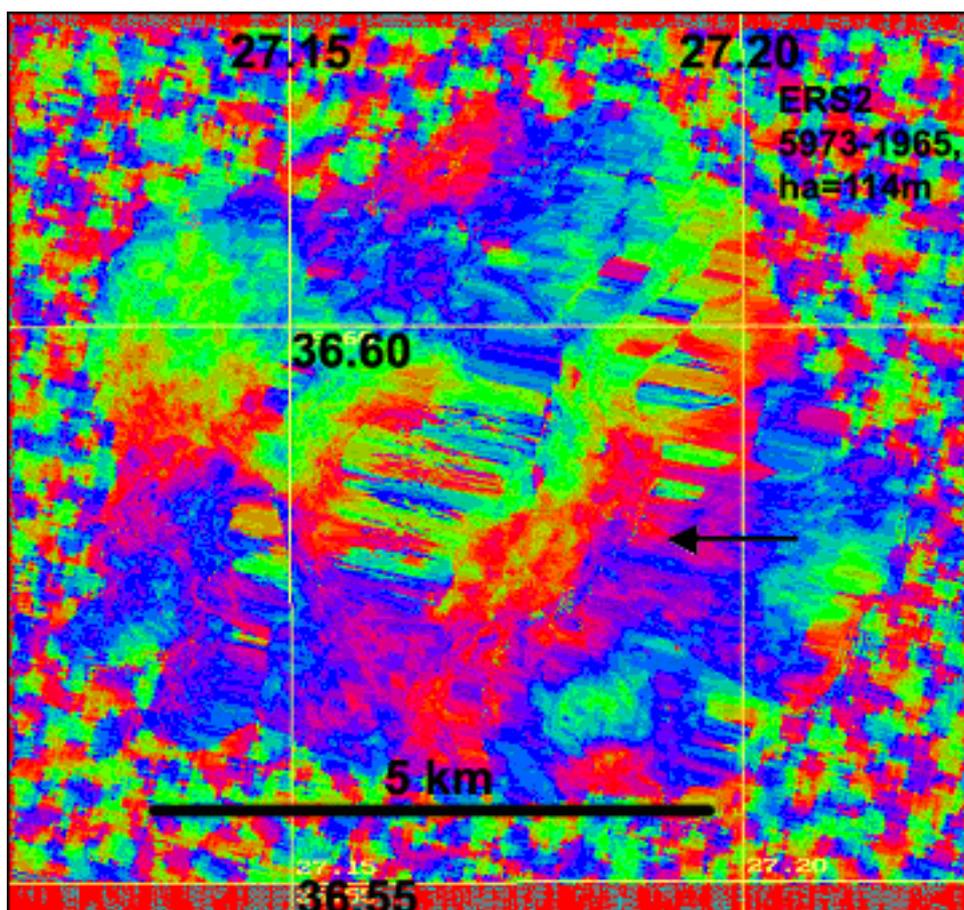
RESULTS

The interferometric phase is shown in Figure 2. Due to the cyclical nature of phase, colour is used to represent it. A zero value is represented by red and as the phase increases it is represented by smooth transition from red to green to blue and then back to red as it reaches 2π (i.e. one cycle). Independent phase effects, which may be present in such an interferogram, are due to topography, surface change and atmospheric anomalies. Because the baseline of

Pair 1 is relatively small (80 m) for ERS the phase is not highly sensitive to the topography (one cycle of phase corresponds to about 117 m in height variation). Despite that the maximum height variation in the region is about 700 m the contribution to the phase due to topography was considered negligible relative to other effects, such as deformation, in the interferogram. This is because topography follows a conic pattern whereas the main fringe trends approximately east-west. There is a significant indication of surface deformation at the study area. A nearly circular phase pattern can be seen in the top near the middle of the scene. Considering the baseline for this InSAR pair this pattern cannot be accounted for by the topography known to be present.

Figure 3. Field photograph of the Nissyros caldera showing the Stefanos crater and the steep slopes of the Profitis Ilias where layover occurs in ERS SAR images during descending orbits. View to the west.
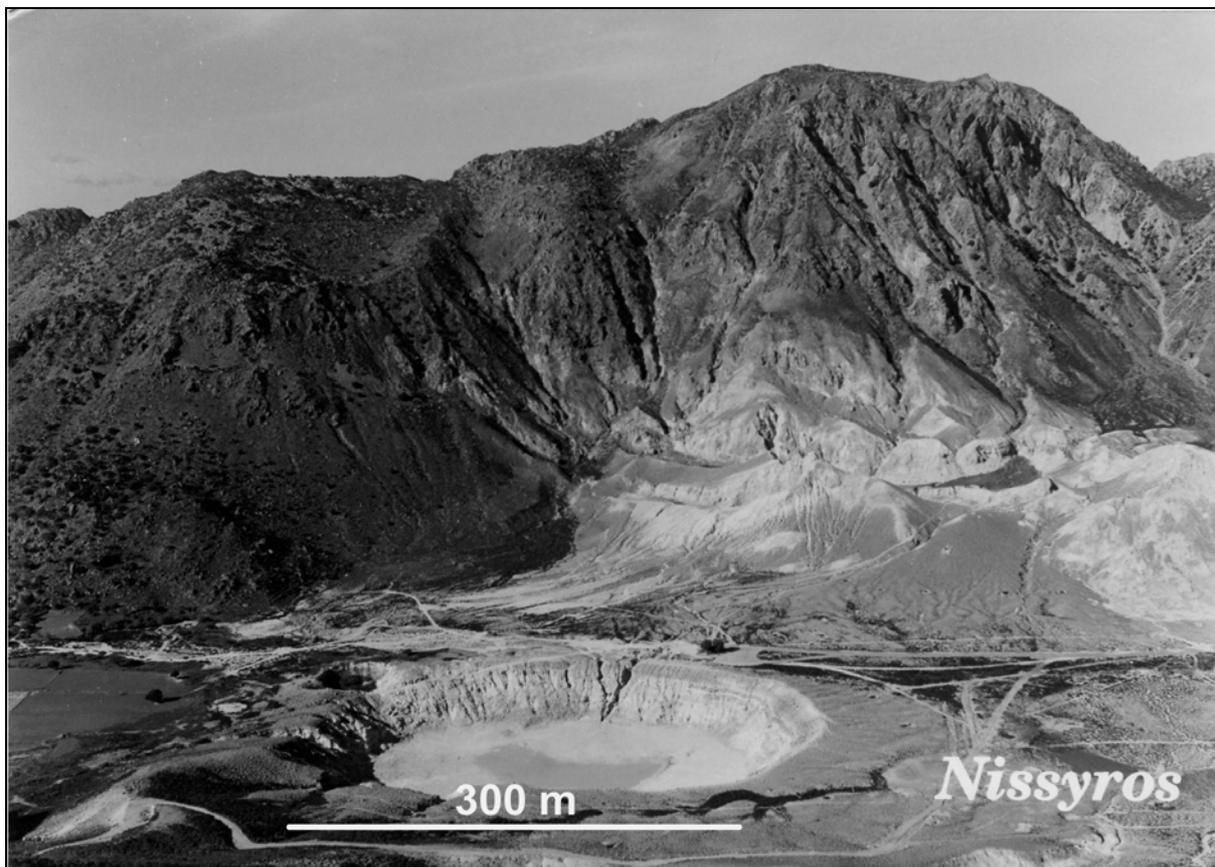
By unwrapping the phase and applying a straightforward conversion a height change map is produced. Note that this conversion assumes that the phase effect measured is due to height change only (no lateral movement). It is important to recognize that the SAR measures only the component of surface motion along the viewing direction of the antenna. The actual surface motion must be inferred from additional knowledge about the area of interest. In the case of the Nissyros volcano, given the relatively conic topography (Figure 3) and the nature of the hydrothermal activities, it is assumed that the surface motion is height change.

DISCUSSION-CONCLUSIONS
The nearly circular feature that can be clearly seen in the Interferogram (Figure 2) is most likely due to uplift. Note that no height change measurements were recovered for most of the bottom of the caldera. This was because the phase

unwrapping failed due to a) prohibitively low coherence and b) geometrical effects (layover of the N-S slopes, i.e. perpendicular to the radar beam). The above results were compared to the pattern of deformation measured by local GPS surveys from 1997 onwards. During the last four years, a series of GPS measurements were made to determine the heights of 14 fixed points distributed throughout Nissyros (Lagios *et al.,* 1998; Lagios, 2000). Analysis of the results provided a preliminary estimate of surface uplift with millimeter accuracy. Comparison of the 1997-1999 survey results to those of the 1995/96 InSAR deformation map is favourable, as the GPS data indicate up to 40mm of uplift. Therefore, areas affected by uplift are clearly evident from the 1995-1996 interferogram.

Figure 4. Seismicity map of the Nissyros area (Data from the NOA National Network). Notice the 2 strong earthquakes of magnitude 5 near the west coast.
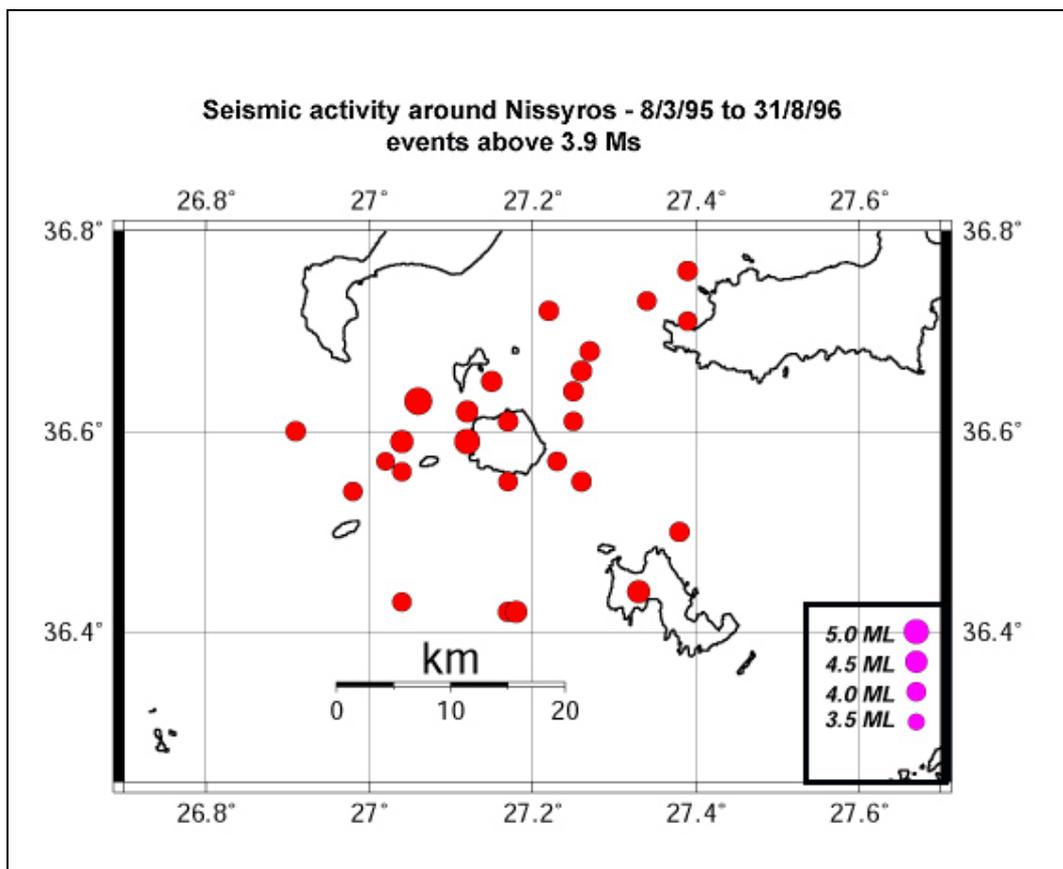
The cause of the 1995-1996 uplift observed by differential InSAR is most probably upward magma movement at the eastern edge of the south Aegean volcanic arc. This movement was accompanied by extensive seismic activity (32 events - Figure 4) which includes two (2) intermediate-depth earthquakes of magnitude 5.5 Ms on 30/11/1995 and 12/4/1996, respectively. This correlation between volcanic and seismic activity has been recently established worldwide by Marzocchi (2002). In the Nissyros case, the triggering mechanism seems to be stress transfer that increased the pressure on the magma chamber. However, most of the earthquakes are shallow (see Appendix) and are concentrated along a NE-WS to E-W general direction which suggests that they occurred within the Kos neotectonic graben (Papanikolaou and Nomikou, 2001). It is worth pointing out that the area of greatest uplift is the northwestern part of the island (which probably includes a significant offshore part) where the destructive, August 1997 earthquake sequence occurred.

Our master SAR scene (11-6-1996) was also used by Parcharidis and Lagios (2001) in their study of the surface deformation of Nissyros. The 3 cm vertical

deformation mapped by our interferogram (Figure 2) was followed during the years 1996-1999 by mostly horizontal movements to the east and southwest, respectively. This change in the mode of deformation could be due to the activation of surface fault zones that cross-cut the volcano.

REFERENCES

[1]Dietrich,. V. J., Kipfer, R. and Schwandner, F. (1998):Mantle-derived noble gases in the South Aegean volcanic arc: Indicators for incipient magmatic activity and deep crustal movements. Newsletter of the European Centre on Prevention and Forecasting of Earthquakes (Council of Europe) 2 (Sept. 1998): 28-32.

[2]Gens, R., 2000. The influence of input parameters on SAR interferometric processing and its implication on the calibration of SAR interferometric data. *Int. J. Remote Sensing*, **21** (8), 1767-1771.

[3]Georgalas, G.C., 1962, Catalogue of the active volcanoes of the world including solfatara fields; Part XII Greece: International Association of Volcanology, Rome, Italy, 40 p.

[4]Lagios E., 2000. Intense crustal deformation rates on Nissyros Island (Greece), deduced from GPS studies, may foreshadow a forthcoming volcanic event. *Proc. 2nd Intern. Conf. On Earthquake Hazard and Seismic Risk Reduction,* Sept. 15-21,1998, Yerevan, Armenia, S. Balassanian et al. (Eds.), Kluwer Academic Publishers, 249-259.

[5]Lagios E., Chailas S., Giannopoulos J. & Sotiropoulos P., 1998. Surveillance of Nissyros Volcano: Establishment and remeasurement of Rn & GPS networks. *Proc. 8th Intern. Congress Geol. Soc. Greece*, Patras, May 27-29, Vol. 32/4, 215-227.

[6]Lanari, R., Lundgren, P., and Sansosti, E., 1998. Dynamic deformation of Etna volcano observed by satellite radar interferometry. *Geophysical Research Letters*, **25** (10), 1541-1544.

[7]Lu, Z., Mann, D., Freymueller, T., and Meyer, D. J., 2000. Synthetic aperture radar interferometry of Okmok volcano, Alaska: Radar observations. J. Geophys. Research, 10791-10806.

[8]Marzocchi, W., 2002. Remote reismic influence on large explosive eruptions. Journal of Geophysical Research, 107 (B1), 1029.

[9]Massonnet, D., Briole, P., and Arnaud, A., 1995. Deflation of mount Etna monitored by spaceborne radar interferometry. *Nature*, **375,** 567-570.

[10]Papadopoulos, G. A., Sachpazi, M., Panopoulou, G., and Stavrakakis, G., 1998. The volcanoseismic crisis of 1996-97 in Nissyros, SE Aegean Sea, Greece. *Terra Nova*, **10**, 151-154.

[11]Papanikolaou, D., and Nomikou, P., 2001. Tectonic structure and volcanic centers at the eastern edge of the Aegean volcanic arc around Nissyros island. *Bulletin of the Geological Society of Greece*, 34(1), 289-296.

[12]Scharroo, R. and P. N. A. M. Visser, and G. J. Mets, 1998. Precise orbit determination and gravity field improvement for the ERS satellites, *J. Geophys. Res*., **103** (C4), 8113-8127.

[13]Parcharidis, I., and Lagios, E., 2001. Deformation in Nissyros volcano (Greece) using Differential radar Interferometry. *Bulletin of the Geological Society of Greece*, 34(4), 1587-1594.

[14]Van der Kooij, M.W.A., Armour, B., Ehrismann, J., Farris-Manning, P., and S. Sato, S., 1997. The EarthView software for Spaceborne Interferometric SAR

processing. *Proceedings 3rd ERS Symposium, (ESA)* 18-21 March 1997 Florence (Italy).

[15]Vassilopoulou, S., and Hurni, L. 2001. The Use of Digital Elevation Models in Emergency and Socio-Economic Planning: A Case Study at Kos – Yali – Nisyros – Tilos Islands, Greece. *Proc. 20th International Cartographic Conference*, Beijing, China, pp. 3424-3431.

APPENDIX. Earthquakes recorded by the National Observatory of Athens (NOA) near Nissyros between 8/3/95 and 31/8/1996 (32 events).

YEAR	M	D	HR	MIN	SEC	LAT	LON	DEP	MAG
1995	MAR	8	08	28	9.3	36.43	27.04	10	3.5
1995	AUG	22	14	26	38.8	36.86	27.41	5	4.0
1995	SEP	11	08	12	59.3	36.60	26.91	32	3.8
1995	NOV	3	20	21	18.9	36.55	27.17	5	3.6
1995	NOV	25	09	04	13.3	36.55	27.26	39	3.7
1995	NOV	25	09	16	39.9	36.61	27.25	37	3.6
1995	NOV	27	13	26	5.2	36.44	27.33	39	4.2
1995	NOV	30	11	49	35.6	36.59	27.12	130	4.8
1995	DEC	14	20	53	24.5	36.50	27.38	5	3.8
1995	DEC	18	07	49	8.4	36.54	26.98	38	3.5
1996	JAN	2	14	54	28.1	36.57	27.02	10	3.4
1996	JAN	2	15	14	36.3	36.56	27.04	10	3.6
1996	JAN	2	20	51	23.8	36.64	27.25	37	3.7
1996	FEB	18	20	03	6.0	36.72	27.22	5	3.7
1996	FEB	29	06	13	21.9	36.76	27.39	37	3.7
1996	APR	8	11	44	59.5	36.65	27.15	33	3.9
1996	APR	12	15	39	12.1	36.63	27.06	153	5.0
1996	APR	25	10	47	39.7	36.85	27.44	1	3.8
1996	APR	25	15	53	3.6	36.89	27.41	1	3.8
1996	APR	25	15	59	58.6	36.89	27.45	10	3.8
1996	APR	27	21	41	51.8	36.68	27.27	10	3.8
1996	APR	30	06	29	7.9	36.73	27.34	10	3.6
1996	APR	30	15	07	23.5	36.66	27.26	10	3.9
1996	MAY	15	06	02	24.4	36.61	27.17	10	3.8
1996	JUN	2	23	52	49.8	36.71	27.39	49	3.6
1996	JUN	26	20	28	37.6	36.57	27.23	5	3.6
1996	AUG	4	18	57	50.6	36.42	27.17	15	3.8
1996	AUG	10	15	23	55.5	36.42	27.18	10	4.0
1996	AUG	19	23	01	35.4	36.62	27.12	5	4.0
1996	AUG	20	15	44	18.4	36.59	27.04	5	4.2
1996	AUG	26	14	01	28.8	36.43	27.11	5	3.6
1996	AUG	31	11	08	37.2	36.59	27.08	5	4.0